UCSF

UC San Francisco Previously Published Works

Title

Distinct neurophysiology during nonword repetition in logopenic and non-fluent variants of primary progressive aphasia

Permalink

https://escholarship.org/uc/item/77g0z3qk

Journal

Human Brain Mapping, 44(14)

ISSN

1065-9471

Authors

Hinkley, Leighton BN

Thompson, Megan

Miller, Zachary A

et al.

Publication Date

2023-10-01

DOI

10.1002/hbm.26408

Peer reviewed

eScholarship.org Powered by the California Digital Library
University of California

Received: 20 December 2022 | Revised: 25 April 2023 | Accepted: 11 June 2023

DOI: 10.1002/hbm.26408

RESEARCH ARTICLE

WILEY

Distinct neurophysiology during nonword repetition in logopenic and non-fluent variants of primary progressive aphasia

Leighton B. N. Hinkley[1] | Megan Thompson[1] | Zachary A. Miller[2] | Valentina Borghesani[2] | Danielle Mizuiri[1] | Wendy Shwe[2] | Abigail Licata[2] | Seigo Ninomiya[1] | Michael Lauricella[2] | Maria Luisa Mandelli[2] | Bruce L. Miller[2] | John Houde[3] | Maria Luisa Gorno-Tempini[2] | Srikantan S. Nagarajan[1]

[1]Department of Radiology and Biomedical Imaging, University of California, San Francisco, California, USA

[2]Department of Neurology, University of California, San Francisco, California, USA

[3]Department of Otolaryngology – Head and Neck Surgery, University of California, San Francisco, California, USA

Correspondence
Leighton B. N. Hinkley, Department of Radiology and Biomedical Imaging, UCSF, 513 Parnassus Avenue S-362, San Francisco, CA 94143, USA.
Email: leighton.hinkley@ucsf.edu

Funding information
Global Brain Health Institute; Larry Hillblom Foundation; National Institutes of Health, Grant/Award Numbers: K23AG048291, K24DC015544, R01AG062196, R01DC013979, R01DC017091, R01DC017696, R01EB022717, R01NS050915, R01NS100440; Ricoh MEG USA; UCOP, Grant/Award Number: MRP-17-454755

Abstract

Overlapping clinical presentations in primary progressive aphasia (PPA) variants present challenges for diagnosis and understanding pathophysiology, particularly in the early stages of the disease when behavioral (speech) symptoms are not clearly evident. Divergent atrophy patterns (temporoparietal degeneration in logopenic variant lvPPA, frontal degeneration in nonfluent variant nfvPPA) can partially account for differential speech production errors in the two groups in the later stages of the disease. While the existing dogma states that neurodegeneration is the root cause of compromised behavior and cortical activity in PPA, the extent to which neurophysiological signatures of speech dysfunction manifest independent of their divergent atrophy patterns remain unknown. We test the hypothesis that nonword deficits in lvPPA and nfvPPA arise from distinct patterns of neural oscillations that are unrelated to atrophy. We use a novel structure–function imaging approach integrating magnetoencephalographic imaging of neural oscillations during a non-word repetition task with voxel-based morphometry-derived measures of gray matter volume to isolate neural oscillation abnormalities independent of atrophy. We find reduced beta band neural activity in left temporal regions associated with the late stages of auditory encoding unique to patients with lvPPA and reduced high-gamma neural activity over left frontal regions associated with the early stages of motor preparation in patients with nfvPPA. Neither of these patterns of reduced cortical oscillations was explained by cortical atrophy in our statistical model. These findings highlight the importance of structure–function imaging in revealing neurophysiological sequelae in early stages of

This is an open access article under the terms of the Creative Commons Attribution-NonCommercial-NoDerivs License, which permits use and distribution in any medium, provided the original work is properly cited, the use is non-commercial and no modifications or adaptations are made.
© 2023 The Authors. *Human Brain Mapping* published by Wiley Periodicals LLC.

dementia when neither structural atrophy nor behavioral deficits are clinically distinct.

KEYWORDS
atrophy, magnetoencephalography, primary progressive aphasia, speech, word repetition

1 | INTRODUCTION

Primary progressive aphasias (PPA) are a category of neurodegenerative diseases characterized by profound declines in linguistic abilities. While diseases of aging with progressive language impairments have been clinically appreciated for over a century, advancements in behavioral neurology have identified three principal PPA variants—semantic variant (svPPA), logopenic variant (lvPPA), and agrammatic/non-fluent variant (nfvPPA). Existing diagnostic criteria (Gorno-Tempini et al., 2011) are based on behavioral presentation, and there are instances where these clinical language presentations can overlap, particularly in the early stages of the disease. It can therefore be difficult for the clinician to differentiate based on behavior alone (Bonner et al., 2010; Gorno-Tempini et al., 2008; Mesulam et al., 2014; Montembeault et al., 2018). The dominant behavioral distinction between the logopenic and non-fluent variants is present during neuropsychological tests of non-word (pseudoword) repetition, where utterances are made that, while meaningless, nevertheless follow the phonological constraints of the patient's native language. While both variants make speech production errors during these tasks, nonword repetition errors are hypothesized to arise from deficits in phonological processing in lvPPA, while errors in nfvPPA are thought to be the result of deficits in motor speech, with lengthened speech duration during this task in the latter group (Ballard et al., 2014). Behaviorally, based on nonword performance errors in lvPPA and nfvPPA as "phonological" versus "motor speech" impairment is however an oversimplification (Eikelboom et al., 2018; Watson et al., 2018), as cognitive impairments beyond language deficits are salient in different PPA subtypes. In the later stages of the disease, these speech errors are associated with neurodegeneration—with temporoparietal atrophy in lvPPA contributing to impaired phonological processing and frontal atrophy in nfvPPA variants contributing to apraxic errors due to impaired motor execution. At the early stages, however, both behavioral errors and atrophy patterns are less differentiated across PPA variants, while functional activation differences between the variants are prominent (Mandelli et al., 2018; Whitwell et al., 2015) suggesting that these deficits in functional activation may act as prominent markers of tracking the disease in its prodromal stages.

We have developed a theoretical framework for explaining the speech repetition deficits in PPA that has at its core our state feedback control (SFC) (Hickok & Poeppel, 2007; Price, 2012; Scott & Johnsrude, 2003) model of speech motor control (Figure 1a). This framework shows how the perceptual, motor and cognitive components of speech converge in the speech repetition task. In the SFC model of the speech motor control system at the heart of this framework, control of the vocal tract is based on estimating and changing the state of the vocal tract articulators. In SFC, the speech motor control system has two key parts: a *controller* that sends controls to the vocal tract articulators, moving them so that the articulatory state (positions and velocities of the articulators) tracks the state sequence

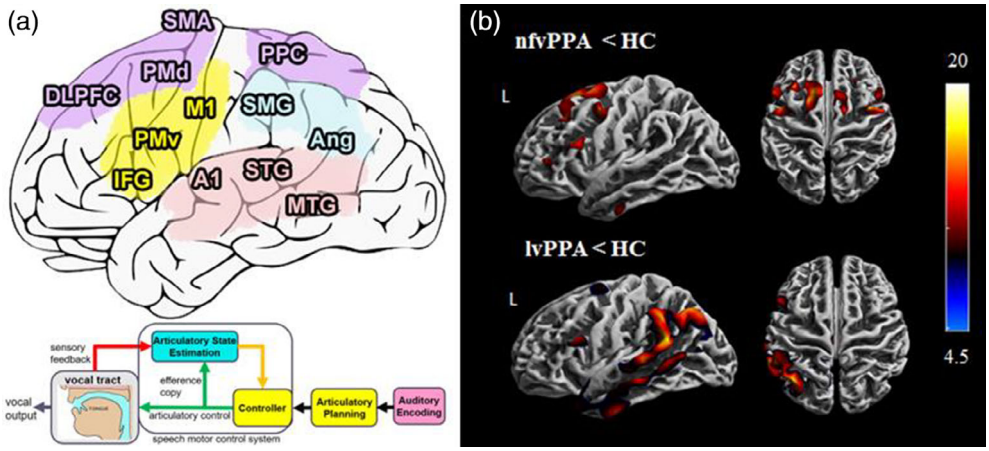

FIGURE 1 (a) A theoretical framework for speech repetition deficits in PPA. Serial models of speech production—in their simplest form—pose a model from auditory encoding in temporal regions (in pink) to speech execution in frontal cortical fields (in yellow). (b) Group level atrophy comparisons between nfvPPA/lvPPA and matched healthy control cohorts showing disease-specific reductions in cortical volume (in red). Although behavioral deficits in PPA map directly on to atrophy in these regions atrophy in PPA also includes regions of association cortex (in blue) that modulate state estimation. Figure B reproduced with permission from Lukic et al. (2019).

needed to produce a desired speech target, and an *articulatory state estimation* process that estimates the state of the vocal tract articulators in two steps: First, it predicts the state that will result from the latest controls acting on the most recent estimate of the articulatory state. Second, it corrects this articulatory state prediction by comparing incoming sensory feedback with predicted feedback, and using the difference to adjust the state prediction so that the sensory feedback it predicts now matches incoming sensory feedback.

Neurophysiological studies in controls using electrophysiological (e.g., ECoG) recordings of these systems demonstrate that oscillatory dynamics underlie these processes across the speech network with functional significance for both linguistic perception and language production (Crone et al., 2001; Edwards et al., 2010; Ojemann et al., 1989). According to these studies, auditory encoding is driven by perception of speech input itself through activation in the superior and middle temporal gyri (STG, MTG) and primary auditory cortices (Figure 1a, in pink). During speech tasks, induced oscillations in the beta (around 30 Hz) and high-gamma (>50 Hz) range over these regions of the temporal lobe are thought to reflect lexical access and phonological processing (Mai et al., 2016; Pulvermuller et al., 1996). In the speech repetition task, these lexical and phonological processes are needed for encoding the speech input into the desired speech targets that the articulatory planning process uses to generate the desired articulatory state sequences that the speech motor control system (the controller and the state estimator) drives the vocal tract to produce (Houde & Nagarajan, 2011; Tourville & Guenther, 2011). These states are computed in frontal motor (inferior frontal gyrus [IFG], ventral pre-motor cortex [PMv], primary motor cortex) regions (Figure 1a, in yellow) where in healthy controls oscillatory dynamics in both beta and high gamma frequency bands are activated during speech tasks (Leuthardt et al., 2012; Zheng et al., 2021) link language perception to motor production for speech articulation (Chang et al., 2011; Haller et al., 2018) Cued speech production tasks like the speech repetition task require not only activation of these aforementioned networks but also input from multiple parallel dorsal frontal–parietal cognitive networks mediating attention, memory and rehearsal (Figure 1a, in purple). Electrophysiological studies done in healthy controls further illustrate that these processes are mediated through task-induced oscillations in the beta and gamma frequency bands (Jensen et al., 2007; Womelsdorf & Everling, 2015).

Studying the neurobiological bases of these functions can be a challenge as they occur rapidly and dynamically change during speech, making them difficult to capture using imaging techniques with reduced temporal capabilities. Furthermore, many of the brain regions that oversee these mediating processes during speech (Figure 1a, in blue) are atrophied (Figure 1b) in both lvPPA and nfvPPA (Lukic et al., 2019). Understanding how oscillations within speech motor cortex operate in PPA variants independent of atrophy patterns can inform us about how regional dysfunction contributes to language deficits and how they contribute to cognitive impairments in PPA more generally, especially in the early stages of the disease.

We use a novel structure–function imaging approach statistically combining task-based imaging with cortical volumetrics in PPA. We test the hypothesis that nonword performance deficits in PPA variants have distinct cortical oscillatory manifestations in the beta and high gamma bands that cannot be explained by neurodegeneration. We reconstruct task-induced neural oscillations during a non-word repetition task using magnetoencephalographic imaging (MEG-I) (Sekihara & Nagarajan, 2015) and combine those reconstructions with voxel-level atrophy values (as covariates) in a structure–function statistical model. Nonword repetition is a commonly used cued task for studying speech processing as it integrates the aforementioned functions of perception, cognition, and action and has been successfully used in studies on patient populations with speech and language deficits (Coady & Evans, 2008). The nonword repetition paradigm additionally induces oscillations in the beta and gamma bands underlying both auditory encoding and speech execution, respectively (Garagnani et al., 2016; Mai et al., 2016). The exquisite spatial and temporal resolution of MEG-I allows us to localize both the timing and frequency components (beta, gamma) of cortical dynamics behind nonword repetition with precision. Merging this data in a multimodal framework with MRI volumetric data registered in the same space allows us to estimate the group differences in neural oscillatory activity that cannot be accounted for by cortical atrophy. Specifically, we predict a spatiotemporal dissociation in neural activation distinguishing the two variants statistically unrelated to atrophy, with impoverished neural oscillations over the left temporal lobe during speech encoding in lvPPA and impoverished oscillations over the left frontal lobe during speech production in nfvPPA. Estimating unique neural deficits during this speaking task that differ between these two variants unaccounted for by atrophy will not only contribute to a better understanding of their underlying pathophysiology but could eventually lead to improvements in differential diagnostic classification between variants utilizing these time-frequency resolved dynamics in the earliest stages of the disease before structural atrophy differences are detectable.

2 | METHODS

2.1 | Participants

All patients (lvPPA, nfvPPA; $n = 22$ in each group) and healthy controls ($n = 18$; Table 1) were recruited through the UCSF Memory and Aging Center (MAC) who met currently published criteria by trained clinicians (medical history, neurological, neuropsychological, and language evaluations (Gorno-Tempini et al., 2011). Individuals with a Mini-Mental State Exam (MMSE) below 13 and/or a Clinical Dementia Rating (CDR) score >1.0 were excluded. All patients underwent a battery of neuropsychological tests (Gorno-Tempini et al., 2004). All participants were group matched for age, gender, and handedness with no significant differences for either continuous (1×3 ANOVA for age, $F_{(2,59)} = 2.89$, $p > .05$) or categorical (Fisher's 2×3 exact test, $p > .05$ for gender and handedness). The study was approved by the UCSF Committee on Human Research and all participants provided written informed consent.

TABLE 1 Study participants demographics.

	n	CDR box	MMSE	Age	Gender	Handedness
Healthy control (HC)	18			70.4	4M/14F	4L/14R
Non-fluent variant PPA (nfvPPA)	22	1.32 (0.26)	27.4 (0.5)	65.9	10M/12F	4L/18R
Logopenic variant PPA (lvPPA)	22	3.37 (0.28)	21.0 (1.2)	66.0	10M/12F	2L/20R

Note: Study participants demographics characteristics of the healthy control (HC), logopenic variant PPA (lvPPA), and non-fluent variant PPA (nfvPPA) cohorts. All participants were matched across the cohorts for age, gender, and handedness. Standard error of the mean in parentheses.
Abbreviations: CDR, clinical dementia rating; MMSE, mini-mental state exam.

2.2 | Study design

2.2.1 | MRI acquisition and preprocessing

For each participant, a high-resolution anatomical MRI was acquired (3.0 T Siemens Trio; MPRAGE; 160 1 mm slices, FOV = 256 mm, TR = 2300 ms, TE = 2.98 ms). MRI scans were acquired, on average, within 3 months before or following MEG data acquisition (mean- = 57 days, SE = 20 days). For atrophy correction all MRIs were prepared using standardized voxel-based morphometry preprocessing steps implemented in SPM8 (tissue segmentation, bias correction, and spatial normalization). Gray matter value in each voxel was multiplied by the Jacobian determinant derived from the spatial normalization and spatially smoothed (8 mm FWHM) and a general linear model was performed to detect differences specifically in gray matter volume between the lvPPA and nfvPPA cohorts and healthy controls.

2.2.2 | MEG acquisition, preprocessing, and source reconstruction

MEG data were collected from each participant using a whole-head 275 axial gradiometer MEG system with third-order gradient correction (MEG International Services Ltd. (MISL), Coquitlam, BC, Canada) at a sampling rate of 1200 Hz. Three fiducial coils (nasion, left/right preauricular) were placed to localize the position of the head relative to the sensor array. All participants engaged in a non-word repetition (NWR) task during MEG scanning (Hinkley, de Witte, et al., 2020) where they were presented as auditory stimulus (nonword) at the beginning of each trial and instructed to repeat back the word that they hear into the microphone. Stimuli consisted of 100 non-words (50 words repeated once) derived from a set of nouns using letter substitutions respecting English phonotactical rules (Table 2). All MEG datasets were pre-processed (excluding noisy sensors/trials with sensor artifacts exceeding 10 pT) before source-space analysis. Trials with no responses and clear false starts were removed from the datasets. Following preprocessing, datasets were reconfigured into a stimulus-locked format (auditory nonword stimulus = 0 ms) representing the auditory encoding phase and a response-locked format (vocal response = 0 ms) representing the response preparation phase.

MEG sensor data were reconstructed in source space using a time-frequency optimized adaptive spatial filtering technique implemented in the Neurodynamic Utility Toolbox for MEG (NUTMEG; http://www.nitrc.org/projects/nutmeg). This algorithm utilizes a beamforming technique to solve the M/EEG inverse problem by generating a lead field of voxels derived from an individual subject's T1-weighted anatomical MRI and fitting M/EEG measurements to this matrix thereby reconstructing the data in source space (Dalal et al., 2008; Sekihara et al., 2001). This technique has reliably been shown to capture task-induced (non-phase locked) changes in oscillatory activity known to be underlying complex cognitive functions, including speech (Chang et al., 2011; Hinkley, de Witte, et al., 2020). From the participant's native MRI space, different sets of weights are computed from each possible location in this grid to estimate that location's contribution to the source solution. Raw MEG sensor data was passed through several filter banks (beta [12–30 Hz], low gamma [30–55 Hz], high-gamma [65–90 Hz], and ultra-high gamma [90–115 Hz] bands) partitioned into partially overlapping time windows (300 ms beta, low gamma; 100 ms high/ultra high gamma; 50 ms step size) optimized for localizing spectral peaks in the MEG data (Hinkley, Dale, et al., 2020). Tomographic volumes of source locations (voxels, 8 mm lead field) were generated through computation of frequency-specific covariance matrices and weights of each location relative to the signal of the MEG sensors. Source power for each location was derived through a noise-corrected pseudo-F statistic expressed in logarithmic units (decibels; dB) comparing signal magnitude during an "active" experimental time window versus a baseline "control" window. From these volumes, a pseudo-F statistic was obtained for each voxel, time window, and frequency band. Frequency bands (beta, high gamma, ultra-high gamma) were chosen in our analyses given the prominent role that they play in cortical engagement during speech reception and production in MEG (Hashimoto et al., 2017; Passaro et al., 2011).

TABLE 2 Psycholinguistic characteristics of nonwords.

N	96
Examples	vicket, lant, cag
Word length	4.74 (3:7)
Orthographic neighbors	6.32 (5.5)
Phonological neighbors	14.86 (13.2)

Note: Psycholinguistic characteristics of NWR stimuli. Values shown include range (Word Length) and standard deviation (Orthographic/Phonological Neighbors).

2.3 | Statistical analysis

Within-subject group analyses (one-sample *t*-test) were evaluated at the voxel level using existing parametric embedded in NUTMEG (Hinkley, Dale, et al., 2020). Between-group (lvPPA vs. HC, nfvPPA vs. HC) analyses comparing differences in oscillatory power from MEG-I reconstructions corrected for measures of gray matter (GM) cortical atrophy from MRI segmentation were performed using the Nutmeg Atrophy Statistics (NAS) extension for NUTMEG (https://www.nitrc.org/projects/nutmeg/). NAS consists of a series of custom multimodal parametric tools allowing statistical correction of MEG-I data from anatomical (MRI) information by registering this data in the same space and computing statistics at the voxelwise level (Figure 2). Registration and re-scaling of both MEG-I reconstructions and VBM datasets in the same space/dimensions allow us to enter values from these measurements at the same location (voxel) into our statistical model. The statistical model (ANCOVA) embedded in NAS permits evaluation of statistically significant differences in a dependent variable measurement (MEG-I) between levels of a categorical independent variable (group) while controlling for a continuously scaled nuisance variable (GM intensity) at each voxel in these registered maps.

For VBM, NAS utilizes DARTEL tools in SPM12 (https://www.fil.ion.ucl.ac.uk/spm/software/spm12/) to prepare segmented maps (gray matter, white matter) for multimodal analysis. MEG-I and GM datasets are prepared in parallel. For MEG-I, time-frequency reconstructions in each subject are spatially normalized to an MNI template using the transformation matrix derived from spatial normalization of the T1-weighted image in SPM. For GM maps, T1-weighted MRIs are preprocessed using the DARTEL pipeline (Ashburner, 2007) and segmented into tissue types. GM maps are spatially normalized to a custom group template ($n = 100$, matched for age, sex, gender, scanner type) in MNI space, and then coregistered and resliced using the same FOV and dimensions as the spatially normalized MEG-I images ($79 \times 95 \times 68$ matrix, 2 mm resolution, smoothed 8 mm FWHM) using tools in SPM12. With the MEG-I and GM maps aligned, group statistics in each voxel are run using a parametric analysis of covariance (ANCOVA) general linear model (https://www.mathworks.com/matlabcentral/fileexchange/27014-mancovan). In our analysis, group effects (differences between HC and lvPPA, HC and nfvPPA) are computed at each voxel location by setting group type (HC, lvPPA, nfvPPA) as our categorical independent variable and oscillatory power values in each voxel from the registered MEG-I maps (in dB) as the predicted variable, while controlling for GM intensity (derived from the coregistered GM maps derived from the DARTEL pipeline) by setting those values as a covariate/nuisance variable. *F*-values reflect group differences in MEG-I oscillatory power (main effects) statistically significant even after GM values in the same voxel (covariate) is taken into account. Corrections for multiple comparisons from the resulting atrophy-corrected statistical maps are then performed using cluster thresholding statistics (Hinkley, Dale, et al., 2020) where a cluster of *k* contiguous voxels surviving a conservative alpha level are chosen for significance. Here, we used a threshold selected to be robust ($p < .025$, $k = 50$) against false positives (Eklund et al., 2016).

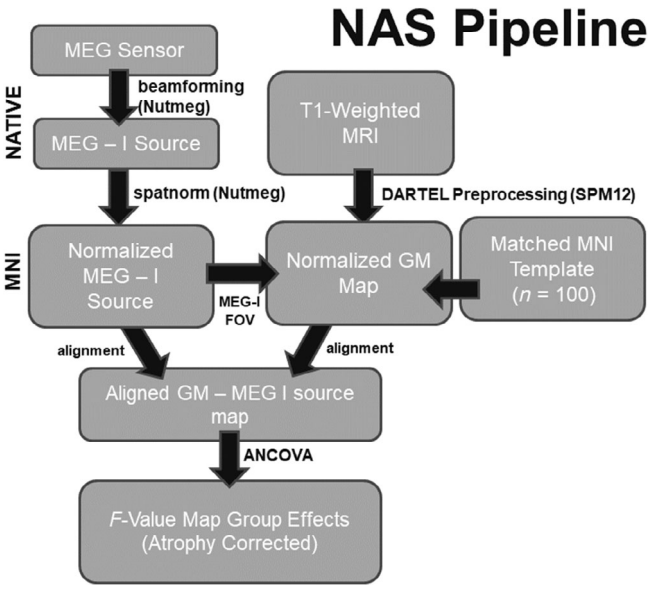

FIGURE 2 Workflow schematic of the NUTMEG Atrophy Statistics (nas) Pipeline for atrophy corrected MEG-I data. Details for this pipeline are provided in Methods section (Section 2.3).

3 | RESULTS

3.1 | Neurophysiological deficits in lvPPA and nfvPPA

Differences (two-tailed unpaired *t*-test) between the lvPPA and nfvPPA participants for neuropsychological measures collected outside of the scanner are shown in Table 3. For measures of language function, patients with lvPPA exhibit significantly reduced scores for repetition measures (WAB, $p < .0001$; Modified Bayles Sentence, $p < .0001$) and picture naming (Boston Naming, $p = .0066$) while nfvPPA participants showed significant increases in both apraxia of speech (AOS, $p < .0001$) and dysarthria ($p = .0005$). No significant differences in measures of visuospatial function were observed between the two cohorts. Lower measures in tests of episodic memory were statistically significant (at $p < .05$) for all measures excluding recognition hits (Table 3). No significant differences were found in any measures of executive function and working memory (Table 3), These observations are consistent with previously published observations in the disorders (Gorno-Tempini et al., 2011) with deficits in repetition and picture naming in lvPPA while patterns of apraxia/dysarthria were present in nfvPPA.

3.2 | Cortical atrophy in lvPPA and nfvPPA

Patterns of cortical atrophy were also consistent with previous reports (Lukic et al., 2019) of cortical volume reduction in inferior

TABLE 3 Neuropsychological testing data from logopenic and non-fluent variant cohorts.

Characteristic	nfvPPA	lvPPA	*p*
Language function			
Apraxia of speech	2.7	0.2	*.0001*
WAB repetition	91.4	75.1	*.0001*
Modified Bayles sentence repetition	0.92	0.62	*.0001*
Dysarthria rating	1.7	0	*.0005*
Long syntax comprehension (%)	0.88	0.80	>.05
Short syntax comprehension (%)	1.00	0.96	>.05
Boston naming test	13.7	10.6	*.0066*
Semantic fluency (animals/min)	13.9	10.9	>.05
Visuospatial function			
CATS face matching	11.4	11.4	>.05
Benson copy	15.0	13.9	>.05
VOSP number location	8.73	8.25	>.05
Episodic memory function			
Benson delayed recall	11.1	7.9	*.0299*
CVLT-MS (30 s delay)	6.86	3.94	*.0024*
CVLT-MS (10 m delay)	6.27	3.67	*.0088*
CVLT recognition hits	8.41	8.33	>.05
Executive function and working memory			
Design fluency: # Correct	7.05	6.06	>.05
Design fluency: # Repeated	1.68	1.17	>.05
Phonemic fluency (D-Words/min)	7.27	7.76	>.05
Modified trails time	20.8	12.8	>.05

Note: Categories of specific neuropsychological tests are labeled in italics.

frontal regions in nfvPPA and temporoparietal regions in lvPPA. In our cohorts, compared with healthy controls, nfvPPA participants show statistically significant reductions in left frontal regions and lvPPA participants show statistically significant reductions in left temporal regions (Figure 3).

3.3 | Increased error and decreased RT during NWR task

Reaction times and error rates (% correct) from the NWR data collected during MEG scanning are shown in Table 4. Reaction times were derived from markers in the MEG dataset from stimulus channel onset to response (microphone, ADC channel) onset in all participants. In a subset of these patients ($n = 15$ HC, $n = 19$ nfvPPA, $n = 16$ lvPPA) correct responses were additionally scored from audio recordings collected during scans and averaged across ratings from three independent trained evaluators. Significant increases in reaction time (compared with healthy controls) were only observed for participants in the nfvPPA cohort ($p = .0026$). Both patient groups exhibited decreased % correct trials (nfvPPA, $p = .0001$; lvPPA, $p = .0001$) when compared with HC. No significant differences were observed between the two groups (lvPPA vs. nfvPPA) in either RT ($p = .15$), accuracy ($p = .91$) or speech duration ($p = .15$).

3.4 | Reduced temporo-parietal oscillatory power in the beta (12–30 Hz) band in lvPPA

Results from both the within-group (one-sample *t*-test) and between group (voxelwise ANCOVA) analyses of beta (12–30 Hz) power change are shown in Figure 4 for both stimulus- and response-locked analyses of the NWR task. Significant ($p < .05$ FWE) reductions in beta power representing underlying neural activity are observed following stimulus presentation across several cortical fields (Figure 4a). In the left hemisphere of the HC cohort, beta activation can be initially observed across the inferior pre-central gyrus (PreCG; 250 ms), followed by the lingual gyrus and fusiform (350 ms), then MTG and posterior parietal cortex (PPC, 450 ms) and finally peaking in the pre-central gyrus (PreCG) at the later stages of stimulus encoding (550 ms). When the control group is compared with the lvPPA group and adjusted for grey matter volume, patients with lvPPA show significantly ($p < .025$ cluster corrected) weakened beta activation over temporal regions, including the left anterior MTG (aMTg; $F_{1,38} = 5.72$, $p = .022$), posterior middle frontal gyrus (pMFg; $F_{1,38} = 10.5$,

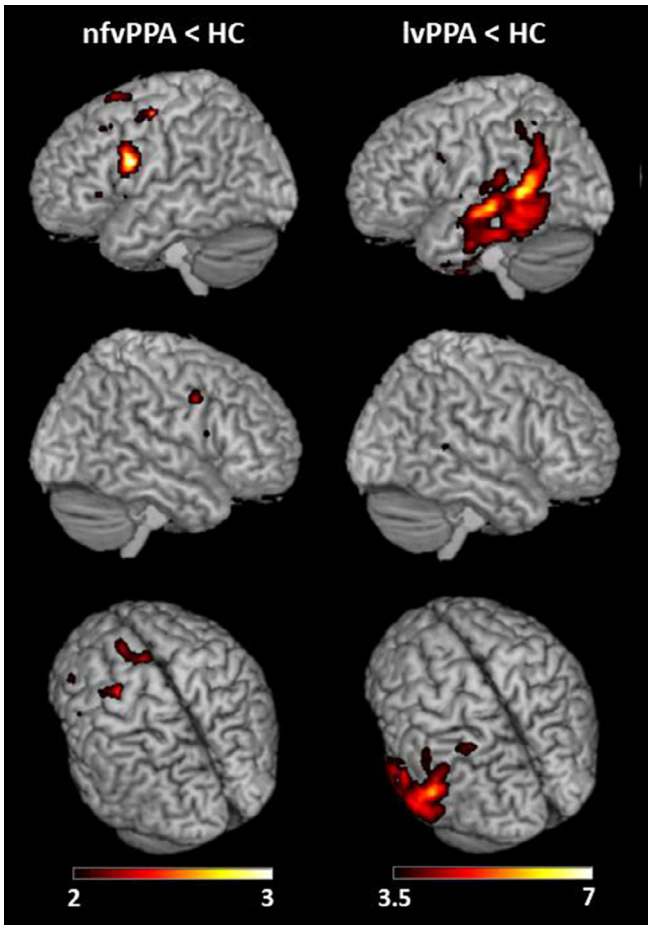

FIGURE 3 Statistically significant reductions of cortical volume (in hot colors) in nfvPPA and lvPPA cohorts (compared with HCs) derived from segmented T1-weighted images prepared using the VBM pipeline. All maps are statistically thresholded and superimposed on rendered brains using MRICro.

TABLE 4 MEG task performance.

	% corr	RT (ms)	Duration (ms)
HC	86.4 (1.7)	1018 (42)	396 (12)
lvPPA	64.9 (3.1)***	1151 (53)	395 (8)
nfvPPA	65.5 (3.8)***	1277 (68)***	417 (13)

Note: Within-scan behavioral performance during the MEG NWR task. Percentage accuracy, reaction time (RT), and response duration scores in all three cohorts. Values shown include standard error of the mean.
***$p < .005$.

$p < .001$) dorsal motor cortex (dMC; $F_{1,38} = 5.49$, $p = .025$) and right inferior frontal (IFt; $F_{1,38} = 7.75$, $p = .008$) regions in the first few hundred milliseconds following stimulus presentation and over left posterior inferior temporal gyrus (pITg; $F_{1,38} = 7.64$, $p = .009$) and inferior temporo-occipital (ITo; $F_{1,38} = 12.01$, $p = .021$) regions later on (Table 5). A similar pattern is seen in the response-locked analysis (Figure 4b), with significant activation over the left speech and language network in all three groups, and in lvPPA, insufficient beta activity ($p < .025$ cluster corrected) over left aMTG ($F_{1,38} = 9.03$, $p = .005$), ITo ($F_{1,38} = 9.31$, $p = .004$) and posterior STG (pSTG; $F_{1,38} = 9.47$, $p = .004$) and robustly over left MTG (pMTG; $F_{1,38} = 15.58$, $p < .001$) before response onset, even when corrected for atrophy. No significant beta activation differences are identifiable between the control and nfvPPA groups (Figure S1) specifying that even when atrophy is taken into account beta oscillations over the left temporal lobe are weaker during later time windows of speech encoding only in lvPPA patients. Decreased beta oscillations are also seen when the lvPPA group is contrasted against the nfvPPA group using the same analyses (Figure S1) indicating that this decreased power is only identifiable in the lvPPA cohort.

In the lvPPA versus HC atrophy corrected comparison, significant ($p < .025$ cluster corrected) increases in beta activity (increased beta power reduction, Figure 4) are observed in both hemispheres (Table 5). For stimulus-locked (Figure 4a), increases in the lvPPA group included the left hemisphere the posterior supramarginal gyrus (pMSg; $F_{1,38} = 11.59$, $p = .002$) and anterior MFG (aMFg; $F_{1,38} = 6.99$, $p = .019$). In the right hemisphere, increases in the lvPPA group included the cerebellum (Cb; $F_{1,38} = 13.33$, $p < .001$), angular gyrus (Ag; $F_{1,38} = 8.25$, $p = .007$), pSMG ($F_{1,38} = 9.71$, $p = .004$), aMFG ($F_{1,38} = 6.99$, $p = .019$) right superior frontal gyrus along the midline (SFg; Cb; $F_{1,38} = 7.17$, $p = .011$). For response locked, increased patterns of beta suppression were statistically significant for the same regions before response onset (Figure 4b, Table 5). These right hemisphere increases were also identified when the lvPPA group is contrasted against the nfvPPA cohort as a control group (Figure S1). No significant increases in beta activation were observed in the nfvPPA versus HC comparison (Figure S1), indicating only lvPPA patients showed both reductions in left temporal beta activation and increases in right frontal–parietal beta activity unrelated to cortical atrophy.

3.5 | Similar oscillatory power in the high gamma (65–90 Hz) band

In the high frequency (65–90 Hz) band during the stimulus encoding and response generation phases of the NWR task (Figure 5) all three groups show significant ($p < .01$ cluster corrected) high-gamma power increases bilaterally over the superior temporal sulcus (STS) 150 ms following stimulus presentation. No significant differences between the groups were identified in the analysis (data not shown for response-locked NWR analysis). Bilateral STS activation is consistent with these areas being involved in auditory perception and not speech production.

3.6 | Reduced frontal oscillatory power in the ultra-high gamma (90–115 Hz) band in nfvPPA

Across all three cohorts, significant increases in ultra-high gamma activity (90–115 Hz) during stimulus encoding and response preparation were significant ($p < .01$ cluster corrected) across several cortical

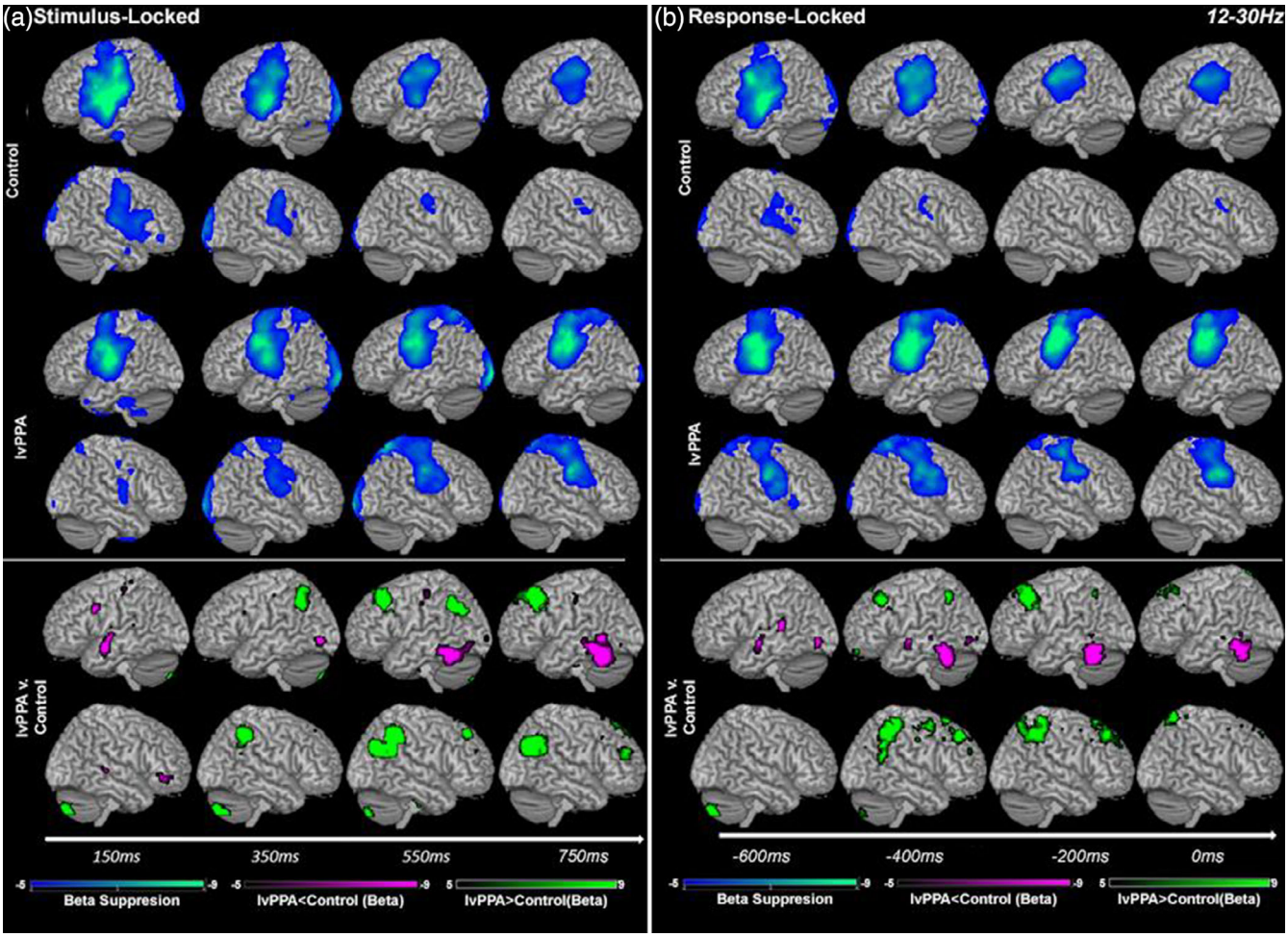

FIGURE 4 Statistically significant patterns of beta frequency (12–30 Hz) neural activation and group differences (lvPPA) for the NWR task (cool colors) and significant between-group atrophy corrected reductions (in violet) and increases (in green) in the lvPPA cohort for the NWR task. (a) Stimulus-locked (0 ms = auditory presentation) analysis. (b) Response-locked (0 ms = vocal response) analysis. Conventions as in previous figures.

fields (Figure 6). In the HC cohort, we see an initial increase in ultra high-gamma activity over the left dorsal pre-motor cortex (PMd) and the supplementary motor area (SMA) 250 ms following stimulus presentation, followed by increases in bilateral occipital-parietal regions (375 ms). In the nfvPPA cohort, ultra-high frequency activation over the dorsal frontal lobe did not survive statistical significance (Figure 6). In the nfvPPA vs. HC atrophy corrected comparison, activation was significantly reduced in nfvPPA (Figure 6a) over the left posterior SMA (pSMA; $F_{1,38} = 6.41$, $p = .045$), posterior PMd (pdPMC; $F_{1,38} = 15.48$, $p < .001$) and ventral pre-motor cortex (vPMC; $F_{1,38} = 10.6$, $p = .002$) with the greatest differences <300 ms following stimulus presentation (Table 5). Additionally, significantly reduced ultra-high gamma power was observed over the left occipital cortex (OC; $F_{1,38} = 16.8$, $p < .001$). A similar pattern was identified in the response-locked analysis, with significantly reduced left frontal ultra-high gamma activation in the nfvPPA cohort during the earliest stages (Table 5) of response preparation (Figure 6b) over the pSMA ($F_{1,38} = 10.6$, $p = .002$), vPMC ($F_{1,38} = 11.0$, $p = .002$), medial dPMC (mdPMC; $F_{1,38} = 6.8$, $p = .013$), bilateral frontal pole (left FP; $F_{1,38} = 12.6$, $p = .001$, right FP; $F_{1,38} = 12.6$, $p = .003$), and anterior MFG (aMFg; $F_{1,38} = 12.0$, $p = .001$). Additional decreases in the nfvPPA cohort localized to left OC ($F_{1,38} = 17.9$, $p < .001$) and superior parietal lobe (SPL; $F_{1,38} = 21.4$, $p < .001$). No differences were identifiable between the HC and lvPPA cohorts (Figure S2) indicating that, while ultra-high oscillations during stimulus encoding and response preparation are preserved in lvPPA, they are significantly weakened in nfvPPA—a pattern not directly accountable by the underlying cortical atrophy. This decrease in both frontal and parietal ultra-high gamma activation was also seen when nfvPPA is contrasted against the lvPPA cohort, indicating that these impoverished left-hemisphere oscillations were specific to nfvPPA and not seen in lvPPA (Figure S2).

4 | DISCUSSION

We sought to determine variant-specific deficits in oscillatory dynamics underlying speech production in lvPPA and nfvPPA that are

TABLE 5 Cluster locations of atrophy-corrected group differences for regions in Figures 3 and 5.

Region	Abbrev	+/−	x	y	z	F	Time	p
Beta (stimulus-locked) lvPPA|HC								
Left anterior middle temporal gyrus	aMTg	−	−50	−9	−2	5.72	250 ms	.022
Left posterior middle frontal gyrus	pMFg	−	−53	10	35	10.5	250 ms	.0003
Left dorsal motor cortex	dMC	−	−52	−25	53	5.49	250 ms	.0245
Right inferior frontal	IFt	−	45	42	−6	7.75	250 ms	.0083
Left posterior inferior temporal gyrus	pITg	−	−21	−99	−13	7.64	750 ms	.0088
Left inferior temporo-occipital	ITo	−	−54	−54	−16	12.01	850 ms	.0013
Right cerebellum	Cb	+	21	−75	−45	13.33	250 ms	.0008
Left posterior supramarginal gyrus	pSMg	+	−50	−59	39	11.59	550 ms	.0016
Right angular gyrus	Ag	+	50	−70	33	8.25	650 ms	.0066
Right anterior middle frontal gyrus	aMFg	+	24	40	47	6.99	750 ms	.0188
Right posterior supramarginal gyrus	pSMg	+	45	−48	47	9.71	850 ms	.0035
Left anterior middle frontal gyrus	aMFg	+	−37	27	44	10.39	850 ms	.0026
Right superior frontal gyrus	SFg	+	7	24	51	7.17	850 ms	.0109
Beta (Response-Locked) lvPPA|HC								
Left anterior middle temporal gyrus	aMTg	−	−59	−8	−8	9.03	−700 ms	.0047
Left inferior temporo-occipital	ITo	−	−48	−81	−8	9.31	−500 ms	.0041
Left posterior superior temporal gyrus	pSTg	−	−54	−34	15	9.47	−500 ms	.004
Left posterior middle temporal gyrus	pMTg	−	−52	−55	−17	15.58	−300 ms	.0003
Right cerebellum	Cb	+	22	−76	−44	10.87	−600 ms	.0021
Left posterior supramarginal gyrus	pSMg	+	−43	−57	50	7.11	−400 ms	.0112
Right anterior middle frontal gyrus	aMFg	+	31	40	48	5.75	−300 ms	.022
Left anterior middle frontal gyrus	aMFg	+	−35	−24	48	6.12	−200 ms	.0179
Right superior frontal gyrus	SFg	+	8	22	48	7.9	−100 ms	.0078
Right posterior supramarginal gyrus	pSMg	+	42	−46	54	8.38	−300 ms	.0063
Ultra High Gamma (Stimulus-Locked) nfvPPA|HC								
Left posterior supplementary motor area	pSMA	−	−2	−12	64	6.41	175 ms	.0156
Left posterior-dorsal premotor cortex	pdPMC	−	−32	−16	64	15.48	225 ms	.0003
Left ventral premotor cortex	vPMC	−	−60	−4	22	10.6	275 ms	.0024
Left occipital cortex	OC	−	−81	−81	24	16.84	475 ms	.0002
Ultra High Gamma (Response-Locked) nfvPPA|HC								
Left posterior-dorsal premotor cortex	mdPMC	−	−28	−19	68	10.63	−825 ms	.0024
Left ventral premotor cortex	vPMC	−	−58	−22	30	11.03	−825 ms	.002
Left posterior supplementary motor area	pSMA	−	−4	−22	74	6.8	−725 ms	.0130
Right frontal pole	FP	−	45	11	49	12.56	−725 ms	.0011
Left frontal pole	FP	−	−34	65	13	10.19	−725 ms	.0028
Right anterior middle frontal gyrus	aMFg	−	45	11	49	12.01	−725 ms	.0013
Left superior parietal lobe	SPL	−	−18	−74	47	21.37	−575 ms	<.0001
Left occipital cortex	OC	−	−21	−85	9	17.91	−575 ms	.0001

Note: Statistically significant differences in oscillatory power in the patient groups are tabulated with respect to cluster location (MNI coordinates) and anatomical label.

dissociable from neurodegeneration, and to examine how well they can be accounted for by our theoretical speech framework. We used a multimodal structure–function imaging approach combining neurodegeneration and functional data. As oscillations are induced across the speech network in both beta and high-gamma bands during nonword repetition tasks, we predicted broadband disruptions of these oscillations over temporoparietal and frontal cortical fields in spatiotemporal patterns unique to each patient group. We identified specific network dysfunction patterns dissociable between the two variants along the dimensions of spatial location, timing, and

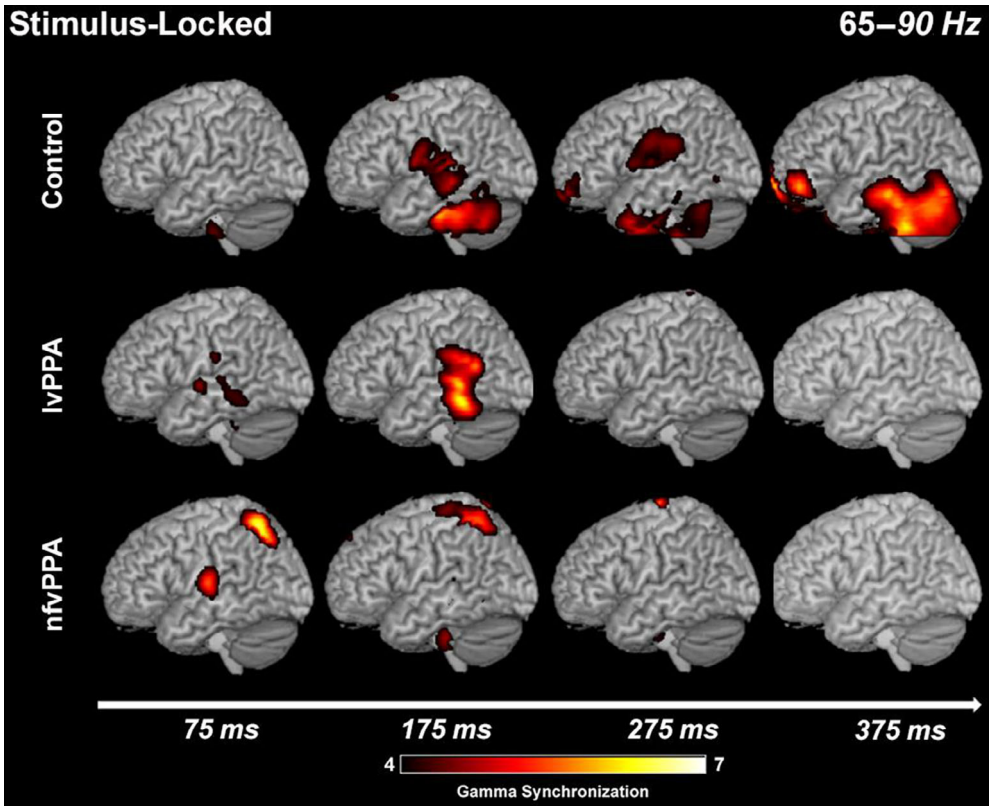

FIGURE 5 Statistically significant patterns of high frequency (65–90 Hz) neural activation (in hot colors) for the NWR task. Stimulus-locked (0 ms = auditory presentation) analysis. Conventions as in previous figures.

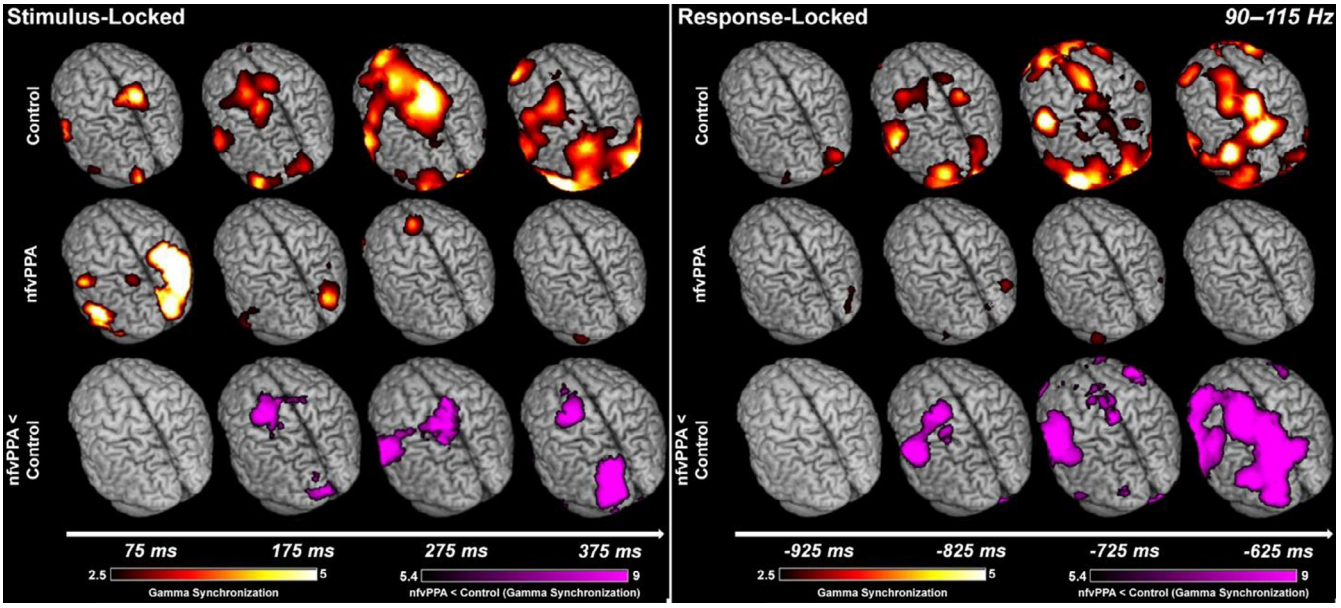

FIGURE 6 Statistically significant patterns of ultra-high frequency (90–115 Hz) neural activation (hot colors) and significant between-group atrophy corrected reductions in the nfvPPA cohort (in violet) for the NWR task. (a) Stimulus-locked (0 ms = auditory presentation) analysis. (b) Response-locked (0 ms = vocal response) analysis. Conventions as in previous figures.

oscillatory frequency band that cannot be accounted for by either difference in neurodegeneration or behavior. Specifically, logopenic variants showed significantly reduced activation over the left posterior temporal lobe late in speech auditory encoding only within low-frequency (beta) bands normally active during healthy controls, consistent with clinical presentation of phonological processing deficits. In contrast, non-fluent variants showed significantly reduced activation over motor association fields during the early stages of speech preparation only in high-frequency (high-gamma) bands typically active during nonword repetition in healthy controls, consistent with

clinical presentation of motor planning deficits (apraxia of speech). These unique cortical oscillatory patterns provide a mechanistic basis for differential clinical sequelae characteristic of the two variants that extend beyond cortical atrophy patterns.

4.1 | Impoverished beta oscillations over temporoparietal regions in lvPPA during auditory encoding accounts for phonological processing deficits

In functional neuroimaging of healthy controls, patterns of cortical activation during pseudoword repetition overlap strongly with real-word repetition (Hartwigsen et al., 2013; Newman & Twieg, 2001). In theoretical frameworks of this task, auditory stimulus features encoded in the posterior regions of the temporal lobe (Figure 1a, in pink) are relayed to motor cortical fields serving speech production (Figure 1a, in yellow). Activation within temporal–parietal regions in healthy controls, particularly in lower frequencies, have been associated with access to a word-specific assembly (Pulvermuller et al., 1996) necessary for both phonological processing and lexical access during these tasks (Mai et al., 2016). We identify prominent reductions in this lower frequency activation over these regions in lvPPA, where group differences were prominent in the later time windows of auditory encoding and the early time windows of speech production. While increased activation was observed bilaterally in frontoparietal networks across time windows, reduced activation in only these low-frequency overlapping time windows reflects a deficit at the later stages of stimulus encoding in lvPPA. This finding is consistent with speech production models (Hagoort & Levelt, 2009; Indefrey & Levelt, 2004) that propose typical phonological processing in posterior temporal regions occurs at the latest stages of linguistic processing (Sahin et al., 2009). In lvPPA, neurodegeneration of these regions is thought to interfere with this late-stage phonological processing leading to speech production deficits (Gorno-Tempini et al., 2008). As the posterior temporal lobe (MTG/ITG) acts as a core component of the phonological loop (Papagno et al., 2017) both neurodegeneration and reduced neural activity in this area during nonword repetition could lead to phonological errors during speech production. Differences over these regions being the most prominent in the beta band are also consistent with known phonological deficits in lvPPA and therefore impoverished beta oscillations during nonword repetition reflect phonological processing deficits and errors during the task. As atrophy patterns did not account for these reductions in neural activity, our findings indicate that impoverished late low-frequency temporal neural oscillations act as a physiological signature of lvPPA unaccounted for by neurodegeneration, potentially representing underlying phonological processing deficits.

While significant reductions in beta-band activity were found in the left hemisphere in our lvPPA cohort, increased activation over right fronto-parietal regions in the same frequency band were also identified in that cohort. It is possible that these findings are functionally analogous to the types of activation shifts observed in stroke-related aphasia, where increased contralesional (right hemisphere) activity occurs (Cao et al., 1999; Raboyeau et al., 2008; Rosen et al., 2000). In contrast, it is also likely that this increase in right-hemisphere activity (and a preponderance for right-hemisphere or bilateral representation for language) exists at the earliest stages of the disease prior to large scale neurodegeneration. Hemispheric shifts for language dominance have been previously reported in PPA (Kielar et al., 2018; Miller et al., 2015) suggesting that neurodevelopmental mechanisms of lateralization may cause a differential pattern of disease susceptibility in this population. While it is possible that this activation in regions not normally robustly active in healthy controls may act as a compensatory mechanism in lvPPA, our current sample size did not allow us to test this hypothesis directly.

4.2 | Impoverished high-gamma oscillations over frontal regions in nfvPPA during planning, articulatory control, and state estimation accounts for motor speech deficits

In the nfvPPA cohort, while low-frequency oscillations over temporal regions were comparable to that in healthy controls, high-gamma oscillations typically identified over PMd/SMA in healthy controls were significantly reduced during the early stages of stimulus encoding and response preparation. In speech neuroscience studies derived from studies on healthy controls, increased activation of this network during pseudoword generation specifically may reflect increased articulation demand and therefore direct generation and sequencing of motor plans (Hartwigsen et al., 2013; Xiao et al., 2005). In theoretical frameworks of speech production, articulatory state estimation signals from sensorimotor association regions (Figure 1a, in blue) converge on motor cortical fields (Figure 1a, in yellow) for articulatory planning before speech output. Given nfvPPA activation differences in the high gamma band occurred far before speech onset it likely represents impoverished transient activation over motor association regions linked to response preparation and articulatory planning, not execution. Slowed articulation rate has been suggested to be a reliable predictor of nfvPPA (Cordella et al., 2017). Processing for articulatory planning may occur in early, high-frequency activation of motor regions commonly reported in ECoG studies of word repetition (Leuthardt et al., 2012). These studies have shown early high-frequency activation over frontal motor regions as part of an associative network of activity (Pulvermuller, 2005) activated in parallel with the temporal lobe. High-frequency activation in the frontal lobe can link perceptual linguistic processing to motor output during pseudoword repetition tasks (Chang et al., 2011; Haller et al., 2018) and compromised high frequency activation in the frontal lobe may lead to apraxic errors in nfvPPA. Non-human primate studies have shown that activation in the superficial (feedforward) layers of cortex is represented in high-frequency oscillations (Buffalo et al., 2011; van Kerkoerle et al., 2014) and has been speculated to be compromised in the frontal lobes in neurodegeneration (Hughes & Rowe, 2013). Importantly, gray matter volume in did not contribute to differences in our study, making this observation consistent with existing

hypotheses in nfvPPA where early, feed-forward stages of response preparation and articulatory planning are compromised in the disorder. A lack of high-frequency oscillations over frontal motor association fields that cannot be explained by atrophy can contribute to challenges in state estimation and articulation, leading to both delayed responses and high error rates during this task.

4.3 | Frequency specific abnormalities in PPA variants and relationships to pathology

The lvPPA and nfvPPA variants are known to have distinct pathologies, with AD pathology most common in the former and tauopothies (specifically, FTLD-tau) most common in the latter (Montembeault et al., 2018). Prior investigations in M/EEG suggest that these distinct pathologies map onto the oscillatory dynamics of the underlying cortical networks. More specifically, impoverished temporal beta oscillations have been observed in M/EEG studies of AD (Fernandez et al., 2006; Nakamura et al., 2018; Pijnenburg et al., 2004) and amnestic MCI patients (Fodor et al., 2018; Prieto del Val et al., 2015). Less is known about how high-frequency oscillations are impacted in FTLD-tau, although reduced gamma power and coherence in motor cortex have been observed in some tauopothies (Hughes et al., 2018). When MEG data in the frequency domain is contrasted between tau and AD pathology, disruption of frontal oscillatory networks is more consistent with underlying tau pathology, while disruption of temporal oscillatory networks are more consistent with underlying AD pathology (Sami et al., 2018). Our findings not only compliment these previous studies but build upon them by indicating that these oscillatory abnormalities are not confounded by neurodegeneration and are instead more closely linked to pathology in these patients.

4.4 | Functional activation differences cannot be accounted for by neurodegeneration

Understanding the relationship between anatomy and physiology is complicated, particularly in the context of normal and pathological aging (Johnson et al., 2000; Maillet & Rajah, 2013). While the historical conventional wisdom is that less brain leads to less activation, this is not always the case, leading to several theoretical models (Park & Reuter-Lorenz, 2009; Reuter-Lorenz & Cappell, 2008) detailing why neurophysiological and neuroanatomical factors are by no means directly associated. This is particularly applicable to imaging conditions like PPA, where the current dogma dictates that reduced neural activity (and ensuing behavioral deficits) are the direct result of neurodegeneration. The findings of the present study emphasize the importance of multimodal neuroimaging approaches and structure–function models to understanding these relationships. By directly challenging an assumption of one-to-one mapping between impoverished neurophysiological processes and cortical atrophy, our findings in MEG reinforce the notion that compromised activation is not purely due to cell death, consistent with hypotheses derived from previous investigations combining atrophy with neurovascular signals (e.g., PET/fMRI). An appreciation for these atrophy-independent oscillatory patterns is imperative for understanding diseases like PPA, where behavioral manifestations are known to precede gross cortical atrophy. The extent to which neurodegeneration leads to decreases in the MEG signal (Greenwood, 2007) remains to be seen, and requires large-scale integration of multiple imaging modalities (MRI, MEG, PET) with clinical diagnostics.

4.5 | Limitations and future directions

We acknowledge that our study has a modest sample size, however it is important to note that PPA is a rare disease and task demand in MEG requires participants to be highly compliant, restricting our ability to recruit large elderly samples for our studies. Limited sample size prevents investigation of how cortical rhythms relate to behavioral deficits (e.g., speech errors). Given SNR constraints in MEG-I, we include all trials during the task (including error trials). It would be interesting (with larger samples, increased trials, and detailed behavioral coding) to further study how errors specific to the two variants (Ballard et al., 2014) relate to neural activity. Although dependence on compliant participants creates an ascertainment bias in recruitment (earlier stages of the disease) our results set up predictions about progression in the later stages of the disease that can be confirmed with follow up longitudinal studies. Lastly, anatomical and functional data in subjects were acquired with a separation in time (~2 months). However, this is well within general practice in clinical research, with ADNI-3 protocols requiring annual scanning (Weiner et al., 2017).

Nonetheless, this study is the first of its kind to combine MRI volumetrics directly with MEG-I oscillatory dynamics in a statistical framework to dissociate neurophysiological patterns between PPA variants unaccounted for by neurodegeneration or behavioral differences. These differences in oscillatory signal can provide distinguishing characteristics for markers unique to PPA in its earliest stages. A better grasp of this neurophysiology is critical for differential diagnostic classification and, ultimately, imaging-based biomarkers. As nonword repetition as a behavioral test is used already to distinguish between lvPPA and nfvPPA variants by examining errors, a deeper understanding of how this works at the neural level could inform which behavioral deficits to target (motor speech, phonology) for innovative treatments in speech and language pathology. Our findings demonstrate the potential for multimodal structure–function studies of dementia variants in providing both understanding of the underlying pathophysiology before structural atrophy differences are detectable or clinical sequelae are distinct.

ACKNOWLEDGMENTS

This work was funded by the following National Institutes of Health grants (K23AG048291, R01NS050915, K24DC015544, R01NS100440, R01DC013979, R01DC017696, R01DC017091, R01EB022717, R01AG062196). Additional funds include the Larry Hillblom Foundation, the Global Brain Health Institute, Research contract from Ricoh MEG USA Inc, and UCOP grant MRP-17-454755. These supporting sources

were not involved in the study design, collection, analysis, or interpretation of data, nor were they involved in writing the article or the decision to submit this report for publication.

CONFLICT OF INTEREST STATEMENT

The authors declare no conflicts of interest.

DATA AVAILABILITY STATEMENT

Nas is currently implemented as a standalone toolbox that works with the NUTMEG software package accessible at https://www.nitrc.org/projects/nutmeg/.

ORCID

Leighton B. N. Hinkley https://orcid.org/0000-0001-7024-3532
Maria Luisa Mandelli https://orcid.org/0000-0002-2518-2520
Srikantan S. Nagarajan https://orcid.org/0000-0001-7209-3857

REFERENCES

Ashburner, J. (2007). A fast diffeomorphic image registration algorithm. *NeuroImage*, *38*, 95–113.

Ballard, K. J., Savage, S., Leyton, C. E., Vogel, A. P., Hornberger, M., & Hodges, J. R. (2014). Logopenic and nonfluent variants of primary progressive aphasia are differentiated by acoustic measures of speech production. *PLoS One*, *9*, e89864.

Bonner, M. F., Ash, S., & Grossman, M. (2010). The new classification of primary progressive aphasia into semantic, logopenic, or nonfluent/agrammatic variants. *Current Neurology and Neuroscience Reports*, *10*, 484–490.

Buffalo, E. A., Fries, P., Landman, R., Buschman, T. J., & Desimone, R. (2011). Laminar differences in gamma and alpha coherence in the ventral stream. *Proceedings of the National Academy of Sciences of the United States of America*, *108*, 11262–11267.

Cao, Y., Vikingstad, E. M., George, K. P., Johnson, A. F., & Welch, K. M. (1999). Cortical language activation in stroke patients recovering from aphasia with functional MRI. *Stroke*, *30*, 2331–2340.

Chang, E. F., Edwards, E., Nagarajan, S. S., Fogelson, N., Dalal, S. S., Canolty, R. T., Kirsch, H. E., Barbaro, N. M., & Knight, R. T. (2011). Cortical spatio-temporal dynamics underlying phonological target detection in humans. *Journal of Cognitive Neuroscience*, *23*, 1437–1446.

Coady, J. A., & Evans, J. L. (2008). Uses and interpretations of non-word repetition tasks in children with and without specific language impairments (SLI). *International Journal of Language & Communication Disorders*, *43*, 1–40.

Cordella, C., Dickerson, B. C., Quimby, M., Yunusova, Y., & Green, J. R. (2017). Slowed articulation rate is a sensitive diagnostic marker for identifying non-fluent primary progressive aphasia. *Aphasiology*, *31*, 241–260.

Crone, N. E., Hao, L., Hart, J., Jr., Boatman, D., Lesser, R. P., Irizarry, R., & Gordon, B. (2001). Electrocorticographic gamma activity during word production in spoken and sign language. *Neurology*, *57*, 2045–2053.

Dalal, S. S., Guggisberg, A. G., Edwards, E., Sekihara, K., Findlay, A. M., Canolty, R. T., Berger, M. S., Knight, R. T., Barbaro, N. M., Kirsch, H. E., & Nagarajan, S. S. (2008). Five-dimensional neuroimaging: Localization of the time-frequency dynamics of cortical activity. *NeuroImage*, *40*, 1686–1700.

Edwards, E., Nagarajan, S. S., Dalal, S. S., Canolty, R. T., Kirsch, H. E., Barbaro, N. M., & Knight, R. T. (2010). Spatiotemporal imaging of cortical activation during verb generation and picture naming. *NeuroImage*, *50*, 291–301.

Eikelboom, W. S., Janssen, N., Jiskoot, L. C., van den Berg, E., Roelofs, A., & Kessels, R. P. C. (2018). Episodic and working memory function in primary progressive aphasia: A meta-analysis. *Neuroscience and Biobehavioral Reviews*, *92*, 243–254.

Eklund, A., Nichols, T. E., & Knutsson, H. (2016). Cluster failure: Why fMRI inferences for spatial extent have inflated false-positive rates. *Proceedings of the National Academy of Sciences of the United States of America*, *113*, 7900–7905.

Fernandez, A., Hornero, R., Mayo, A., Poza, J., Gil-Gregorio, P., & Ortiz, T. (2006). MEG spectral profile in Alzheimer's disease and mild cognitive impairment. *Clinical Neurophysiology*, *117*, 306–314.

Fodor, Z., Siraly, E., Horvath, A., Salacz, P., Hidasi, Z., Csibri, E., Szabó, Á., & Csukly, G. (2018). Decreased event-related beta synchronization during memory maintenance marks early cognitive decline in mild cognitive impairment. *Journal of Alzheimer's Disease*, *63*, 489–502.

Garagnani, M., Lucchese, G., Tomasello, R., Wennekers, T., & Pulvermuller, F. (2016). A spiking neurocomputational model of high-frequency oscillatory brain responses to words and pseudowords. *Frontiers in Computational Neuroscience*, *10*, 145.

Gorno-Tempini, M. L., Brambati, S. M., Ginex, V., Ogar, J., Dronkers, N. F., Marcone, A., Perani, D., Garibotto, V., Cappa, S. F., & Miller, B. L. (2008). The logopenic/phonological variant of primary progressive aphasia. *Neurology*, *71*, 1227–1234.

Gorno-Tempini, M. L., Dronkers, N. F., Rankin, K. P., Ogar, J. M., Phengrasamy, L., Rosen, H. J., Johnson, J. K., Weiner, M. W., & Miller, B. L. (2004). Cognition and anatomy in three variants of primary progressive aphasia. *Annals of Neurology*, *55*, 335–346.

Gorno-Tempini, M. L., Hillis, A. E., Weintraub, S., Kertesz, A., Mendez, M., Cappa, S. F., Ogar, J. M., Rohrer, J. D., Black, S., Boeve, B. F., Manes, F., Dronkers, N. F., Vandenberghe, R., Rascovsky, K., Patterson, K., Miller, B. L., Knopman, D. S., Hodges, J. R., Mesulam, M. M., & Grossman, M. (2011). Classification of primary progressive aphasia and its variants. *Neurology*, *76*, 1006–1014.

Greenwood, P. M. (2007). Functional plasticity in cognitive aging: Review and hypothesis. *Neuropsychology*, *21*, 657–673.

Hagoort, P., & Levelt, W. J. (2009). Neuroscience. The speaking brain. *Science*, *326*, 372–373.

Haller, M., Case, J., Crone, N. E., Chang, E. F., King-Stephens, D., Laxer, K. D., Weber, P. B., Parvizi, J., Knight, R. T., & Shestyuk, A. Y. (2018). Persistent neuronal activity in human prefrontal cortex links perception and action. *Nature Human Behaviour*, *2*, 80–91.

Hartwigsen, G., Saur, D., Price, C. J., Baumgaertner, A., Ulmer, S., & Siebner, H. R. (2013). Increased facilitatory connectivity from the pre-SMA to the left dorsal premotor cortex during pseudoword repetition. *Journal of Cognitive Neuroscience*, *25*, 580–594.

Hashimoto, H., Hasegawa, Y., Araki, T., Sugata, H., Yanagisawa, T., Yorifuji, S., & Hirata, M. (2017). Non-invasive detection of language-related prefrontal high gamma band activity with beamforming MEG. *Scientific Reports*, *7*, 14262.

Hickok, G., & Poeppel, D. (2007). The cortical organization of speech processing. *Nature Reviews. Neuroscience*, *8*, 393–402.

Hinkley, L. B. N., Dale, C. L., Cai, C., Zumer, J., Dalal, S., Findlay, A., Sekihara, K., & Nagarajan, S. S. (2020). NUTMEG: Open source software for M/EEG source reconstruction. *Frontiers in Neuroscience*, *14*, 710.

Hinkley, L. B. N., de Witte, E., Cahill-Thompson, M., Mizuiri, D., Garrett, C., Honma, S., Findlay, A., Gorno-Tempini, M. L., Tarapore, P., Kirsch, H. E., Mariën, P., Houde, J. F., Berger, M., & Nagarajan, S. S. (2020). Optimizing magnetoencephalographic imaging estimation of language lateralization for simpler language tasks. *Frontiers in Human Neuroscience*, *14*, 105.

Houde, J. F., & Nagarajan, S. S. (2011). Speech production as state feedback control. *Frontiers in Human Neuroscience*, *5*, 82.

Hughes, L. E., Rittman, T., Robbins, T. W., & Rowe, J. B. (2018). Reorganization of cortical oscillatory dynamics underlying disinhibition in frontotemporal dementia. *Brain*, *141*, 2486–2499.

Hughes, L. E., & Rowe, J. B. (2013). The impact of neurodegeneration on network connectivity: A study of change detection in frontotemporal dementia. *Journal of Cognitive Neuroscience*, *25*, 802–813.

Indefrey, P., & Levelt, W. J. (2004). The spatial and temporal signatures of word production components. *Cognition*, *92*, 101–144.

Jensen, O., Kaiser, J., & Lachaux, J. P. (2007). Human gamma-frequency oscillations associated with attention and memory. *Trends in Neurosciences*, *30*, 317–324.

Johnson, S. C., Saykin, A. J., Baxter, L. C., Flashman, L. A., Santulli, R. B., McAllister, T. W., & Mamourian, A. C. (2000). The relationship between fMRI activation and cerebral atrophy: Comparison of normal aging and Alzheimer disease. *NeuroImage*, *11*, 179–187.

Kielar, A., Deschamps, T., Jokel, R., & Meltzer, J. A. (2018). Abnormal language-related oscillatory responses in primary progressive aphasia. *NeuroImage: Clinical*, *18*, 560–574.

Leuthardt, E. C., Pei, X. M., Breshears, J., Gaona, C., Sharma, M., Freudenberg, Z., Barbour, D., & Schalk, G. (2012). Temporal evolution of gamma activity in human cortex during an overt and covert word repetition task. *Frontiers in Human Neuroscience*, *6*, 99.

Lukic, S., Mandelli, M. L., Welch, A., Jordan, K., Shwe, W., Neuhaus, J., Miller, Z., Hubbard, H. I., Henry, M., Miller, B. L., Dronkers, N. F., & Gorno-Tempini, M. L. (2019). Neurocognitive basis of repetition deficits in primary progressive aphasia. *Brain and Language*, *194*, 35–45.

Mai, G., Minett, J. W., & Wang, W. S. (2016). Delta, theta, beta, and gamma brain oscillations index levels of auditory sentence processing. *NeuroImage*, *133*, 516–528.

Maillet, D., & Rajah, M. N. (2013). Association between prefrontal activity and volume change in prefrontal and medial temporal lobes in aging and dementia: A review. *Ageing Research Reviews*, *12*, 479–489.

Mandelli, M. L., Welch, A. E., Vilaplana, E., Watson, C., Battistella, G., Brown, J. A., Possin, K. L., Hubbard, H. I., Miller, Z. A., Henry, M. L., Marx, G. A., Santos-Santos, M. A., Bajorek, L. P., Fortea, J., Boxer, A., Rabinovici, G., Lee, S., Deleon, J., Rosen, H. J., … Gorno-Tempini, M. L. (2018). Altered topology of the functional speech production network in non-fluent/agrammatic variant of PPA. *Cortex*, *108*, 252–264.

Mesulam, M. M., Rogalski, E. J., Wieneke, C., Hurley, R. S., Geula, C., Bigio, E. H., Thompson, C. K., & Weintraub, S. (2014). Primary progressive aphasia and the evolving neurology of the language network. *Nature Reviews. Neurology*, *10*, 554–569.

Miller, Z. A., Hinkley, L. B., Herman, A., Honma, S., Findlay, A., Block, N., Ketelle, R., Rabinovici, G., Rosen, H., Nagarajan, S. S., Miller, B. L., & Gorno-Tempini, M. L. (2015). Anomalous functional language lateralization in semantic variant PPA. *Neurology*, *84*, 204–206.

Montembeault, M., Brambati, S. M., Gorno-Tempini, M. L., & Migliaccio, R. (2018). Clinical, anatomical, and pathological features in the three variants of primary progressive aphasia: A review. *Frontiers in Neurology*, *9*, 692.

Nakamura, A., Cuesta, P., Fernandez, A., Arahata, Y., Iwata, K., Kuratsubo, I., Bundo, M., Hattori, H., Sakurai, T., Fukuda, K., Washimi, Y., Endo, H., Takeda, A., Diers, K., Bajo, R., Maestú, F., Ito, K., & Kato, T. (2018). Electromagnetic signatures of the preclinical and prodromal stages of Alzheimer's disease. *Brain*, *141*, 1470–1485.

Newman, S. D., & Twieg, D. (2001). Differences in auditory processing of words and pseudowords: An fMRI study. *Human Brain Mapping*, *14*, 39–47.

Ojemann, G. A., Fried, I., & Lettich, E. (1989). Electrocorticographic (ECoG) correlates of language. I. Desynchronization in temporal language cortex during object naming. *Electroencephalography and Clinical Neurophysiology*, *73*, 453–463.

Papagno, C., Comi, A., Riva, M., Bizzi, A., Vernice, M., Casarotti, A., Fava, E., & Bello, L. (2017). Mapping the brain network of the phonological loop. *Human Brain Mapping*, *38*, 3011–3024.

Park, D. C., & Reuter-Lorenz, P. (2009). The adaptive brain: Aging and neurocognitive scaffolding. *Annual Review of Psychology*, *60*, 173–196.

Passaro, A. D., Rezaie, R., Moser, D. C., Li, Z., Dias, N., & Papanicolaou, A. C. (2011). Optimizing estimation of hemispheric dominance for language using magnetic source imaging. *Brain Research*, *1416*, 44–50.

Pijnenburg, Y. A., Made, Y., Van Cappellen van Walsum, A. M., Knol, D. L., Scheltens, P., & Stam, C. J. (2004). EEG synchronization likelihood in mild cognitive impairment and Alzheimer's disease during a working memory task. *Clinical Neurophysiology*, *115*, 1332–1339.

Price, C. J. (2012). A review and synthesis of the first 20 years of PET and fMRI studies of heard speech, spoken language and reading. *NeuroImage*, *62*, 816–847.

Prieto del Val, L., Cantero, J. L., & Atienza, M. (2015). APOE varepsilon4 constrains engagement of encoding-related compensatory networks in amnestic mild cognitive impairment. *Hippocampus*, *25*, 993–1007.

Pulvermuller, F. (2005). Brain mechanisms linking language and action. *Nature Reviews. Neuroscience*, *6*, 576–582.

Pulvermuller, F., Eulitz, C., Pantev, C., Mohr, B., Feige, B., Lutzenberger, W., Elbert, T., & Birbaumer, N. (1996). High-frequency cortical responses reflect lexical processing: An MEG study. *Electroencephalography and Clinical Neurophysiology*, *98*, 76–85.

Raboyeau, G., de Boissezon, X., Marie, N., Balduyck, S., Puel, M., Bezy, C., Démonet, J. F., & Cardebat, D. (2008). Right hemisphere activation in recovery from aphasia: Lesion effect or function recruitment? *Neurology*, *70*, 290–298.

Reuter-Lorenz, P. A., & Cappell, K. A. (2008). Neurocognitive aging and the compensation hypothesis. *Current Directions in Psychological Science*, *17*, 177–182.

Rosen, H. J., Petersen, S. E., Linenweber, M. R., Snyder, A. Z., White, D. A., Chapman, L., Dromerick, A. W., Fiez, J. A., & Corbetta, M. (2000). Neural correlates of recovery from aphasia after damage to left inferior frontal cortex. *Neurology*, *55*, 1883–1894.

Sahin, N. T., Pinker, S., Cash, S. S., Schomer, D., & Halgren, E. (2009). Sequential processing of lexical, grammatical, and phonological information within Broca's area. *Science*, *326*, 445–449.

Sami, S., Williams, N., Hughes, L. E., Cope, T. E., Rittman, T., Coyle-Gilchrist, I. T. S., Henson, R. N., & Rowe, J. B. (2018). Neurophysiological signatures of Alzheimer's disease and frontotemporal lobar degeneration: Pathology versus phenotype. *Brain*, *141*, 2500–2510.

Scott, S. K., & Johnsrude, I. S. (2003). The neuroanatomical and functional organization of speech perception. *Trends in Neurosciences*, *26*, 100–107.

Sekihara, K., & Nagarajan, S. S. (2015). *Electromagnetic brain imaging: A Bayesian perspective*. Springer.

Sekihara, K., Nagarajan, S. S., Poeppel, D., Marantz, A., & Miyashita, Y. (2001). Reconstructing spatio-temporal activities of neural sources using an MEG vector beamformer technique. *IEEE Transactions on Biomedical Engineering*, *48*, 760–771.

Tourville, J. A., & Guenther, F. H. (2011). The DIVA model: A neural theory of speech acquisition and production. *Language & Cognitive Processes*, *26*, 952–981.

van Kerkoerle, T., Self, M. W., Dagnino, B., Gariel-Mathis, M. A., Poort, J., van der Togt, C., & Roelfsema, P. R. (2014). Alpha and gamma oscillations characterize feedback and feedforward processing in monkey visual cortex. *Proceedings of the National Academy of Sciences of the United States of America*, *111*, 14332–14341.

Watson, C. L., Possin, K., Allen, I. E., Hubbard, H. I., Meyer, M., Welch, A. E., Rabinovici, G. D., Rosen, H., Rankin, K. P., Miller, Z., Santos-Santos, M. A., Kramer, J. H., Miller, B. L., & Gorno-Tempini, M. L. (2018). Visuospatial functioning in the primary progressive aphasias. *Journal of the International Neuropsychological Society*, *24*, 259–268.

Weiner, M. W., Veitch, D. P., Aisen, P. S., Beckett, L. A., Cairns, N. J., Green, R. C., Harvey, D., Jack, C. R., Jr., Jagust, W., Morris, J. C., Petersen, R. C., Salazar, J., Saykin, A. J., Shaw, L. M., Toga, A. W., Trojanowski, J. Q., & Alzheimer's Disease Neuroimaging Initiative. (2017). The Alzheimer's disease neuroimaging initiative 3: Continued innovation for clinical trial improvement. *Alzheimer's & Dementia*, *13*, 561–571.

Whitwell, J. L., Jones, D. T., Duffy, J. R., Strand, E. A., Machulda, M. M., Przybelski, S. A., Vemuri, P., Gregg, B. E., Gunter, J. L., Senjem, M. L., Petersen, R. C., Jack, C. R., Jr., & Josephs, K. A. (2015). Working memory and language network dysfunctions in logopenic aphasia: A task-free fMRI comparison with Alzheimer's dementia. *Neurobiology of Aging*, *36*, 1245–1252.

Womelsdorf, T., & Everling, S. (2015). Long-range attention networks: Circuit motifs underlying endogenously controlled stimulus selection. *Trends in Neurosciences*, *38*, 682–700.

Xiao, Z., Zhang, J. X., Wang, X., Wu, R., Hu, X., Weng, X., & Tan, L. H. (2005). Differential activity in left inferior frontal gyrus for pseudowords and real words: An event-related fMRI study on auditory lexical decision. *Human Brain Mapping*, *25*, 212–221.

Zheng, W., Minama Reddy, G. K., Dai, F., Chandramani, A., Brang, D., Hunter, S., Kohrman, M. H., Rose, S., Rossi, M., Tao, J., Wu, S., Byrne, R., Frim, D. M., Warnke, P., & Towle, V. L. (2021). Chasing language through the brain: Successive parallel networks. *Clinical Neurophysiology*, *132*, 80–93.

SUPPORTING INFORMATION

Additional supporting information can be found online in the Supporting Information section at the end of this article.

How to cite this article: Hinkley, L. B. N., Thompson, M., Miller, Z. A., Borghesani, V., Mizuiri, D., Shwe, W., Licata, A., Ninomiya, S., Lauricella, M., Mandelli, M. L., Miller, B. L., Houde, J., Gorno-Tempini, M. L., & Nagarajan, S. S. (2023). Distinct neurophysiology during nonword repetition in logopenic and non-fluent variants of primary progressive aphasia. *Human Brain Mapping*, *44*(14), 4833–4847. https://doi.org/10.1002/hbm.26408